Doping characterization for germanium-based microelectronics and photovoltaics using the differential Hall technique

AIP | Applied Physics Letters

Doping characterization for germanium-based microelectronics and photovoltaics using the differential Hall technique

N. S. Bennett and N. E. B. Cowern

Citation: Applied Physics Letters **100**, 172106 (2012); doi: 10.1063/1.4705293
View online: http://dx.doi.org/10.1063/1.4705293
View Table of Contents: http://scitation.aip.org/content/aip/journal/apl/100/17?ver=pdfcov
Published by the AIP Publishing

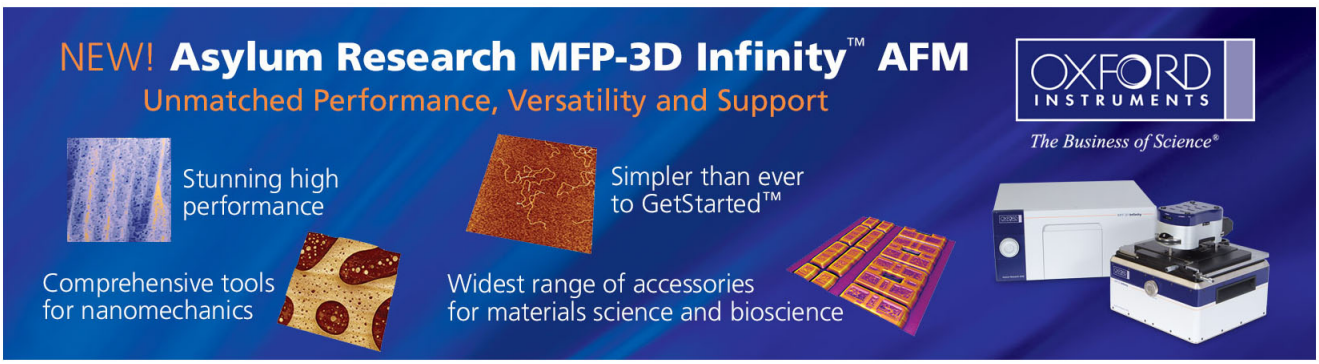

Doping characterization for germanium-based microelectronics and photovoltaics using the differential Hall technique

N. S. Bennett[1,2,a)] and N. E. B. Cowern[1]
[1]*School of Electrical, Electronic and Computer Engineering, Newcastle University, Newcastle upon Tyne NE1 7RU, United Kingdom*
[2]*Nanomaterials Processing Laboratory, School of Electronic Engineering, Dublin City University, Dublin 9, Ireland*

(Received 11 March 2012; accepted 5 April 2012; published online 24 April 2012)

In this coming decade, complementary metal-oxide-semiconductor microelectronic devices may undergo a major change with the implementation of germanium channels. Likewise, the performance of photovoltaic cells based on elemental semiconductors will continue to be optimized. Both technologies will rely on a detailed and thorough understanding of electrical properties, and here, precise doping characterization will play a key role. The differential Hall technique combines resistivity and Hall-effect measurements with successive surface layer removal, allowing one to measure independent carrier concentration and mobility depth profiles. In this Letter, we apply the technique for both microelectronic- and photovoltaic-relevant doping structures in germanium. Controllable and uniform layer removal is achieved with tailored depth resolution (<1–20 nm) for a range of doping structures (30–600 nm). © *2012 American Institute of Physics*. [http://dx.doi.org/10.1063/1.4705293]

Hall-effect and sheet resistivity measurements in combination with layer removal have traditionally been used to measure ion implanted layers in Si microelectronics.[1] The layer removal technique must be controllable with adequate depth resolution and almost constant removal rate over large thicknesses. Recently, anodic oxidation followed by selective oxide removal has been favoured for characterisation of ultra-shallow junctions in Si.[2] A move by the Integrated Circuit industry to Ge channels could present problems for anodic oxidation, since the highly soluble nature of the Ge oxide results in a leaky, non-uniform layer, making it unfit for purpose.[3] Likewise, electrochemical profiling is also troublesome for Ge due to non-availability of a suitable electrolyte.[4] A potential solution is to use slow chemical etching of Ge using H_2O_2 and H_2O. These chemicals produce a slow oxidation of Ge, allowing controllable removal of oxide. The removal process can be tailored for very thin doped layers ($\sim$20 nm) suitable for microelectronics characterization, or for relatively thick total layer removal (>600 nm), more suited to doping metrology for photovoltaics.

In this Letter, etch solutions were prepared by dissolving one part H_2O_2 in ten parts deionised H_2O. The mixture provides a combined mechanism of oxide growth (by Ge reacting with H_2O_2) and removal (the oxide dissolves in H_2O). This particular mixture was chosen based on the findings of Ref. 5 in order to produce a solution with an etch rate which is similar for both n- and p-type Ge, i.e., making it suitable for consistent layer removal across doped junctions. Dedicated etch rate experiments were carried out as a first step to investigate the Ge etch rate and uniformity in B-implanted n-type Ge and P-diffused p-type Ge. Bulk 2 in. n- and p-type wafers were used for this experiment, with constant background doping concentrations of $\sim 10^{17}$ cm^{-3} in each case. B implantation was carried out using an implant energy of 500 eV and dose of 10^{15} cm^{-2} following pre-amorphisation using a 40 keV, 10^{15} cm^{-2} Ge ion implant. This implant condition was chosen to replicate in one dimension an ultra-shallow junction implant for microelectronic devices. To imitate doping structures used in photovoltaics, in this case, the n+ emitter structure, P was introduced to the surface of Ge wafers by application of a commercially available spin-on-dopant (SOD). In the case of ion implanted samples, rapid thermal annealing was carried out at 600 °C for 100 s in nitrogen. For the SOD, P was diffused into the bulk using a 600 s furnace anneal at 600 °C. Secondary ion mass spectrometry (SIMS) was carried out to measure chemical doping profiles for both the ultra-shallow and deep doping structures using either a Cs or O incident beam. A SIMS profile for each doping structure is illustrated in Fig. 1.

Etch experiments were carried out with the etch solution at room temperature and with continual agitation of the wafer pieces. Each test piece was partially covered with photoresist, which following the etch experiment, was then removed using acetone—which does not react with Ge or Ge oxide[5]—to reveal a non-etched surface adjacent to the etch crater. Etched regions were then measured relative to masked regions to determine the etch rate. Etch pits were analysed using a stylus profilometer and were measured over a lateral range of tens of microns. The profilometer results were validated on selected samples using atomic-force microscopy. Each etch crater was measured at $\geq$3 locations to investigate etch uniformity. Additionally, a number of sacrificial samples were etched without electrical measurements, simply to investigate the etch procedure and test its repeatability. The error bar associated with sample-to-sample variation is encapsulated within each data symbol in Fig. 2, where results for the etching experiment are presented. Fig. 2 demonstrates a reasonably uniform and controllable etch rate for both

a)Electronic mail: nick.bennett@dcu.ie.

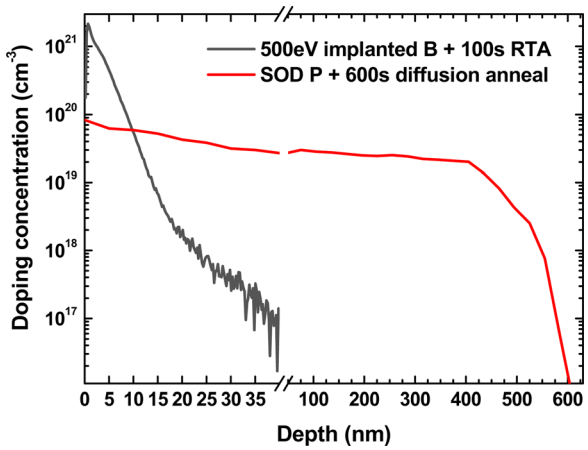

FIG. 1. SIMS profiles for (grey) 500 eV, 10^{15} cm^{-2} B ion implant in n-type Ge, following 40 keV, 10^{15} cm^{-2} Ge pre-amorphizing implant and annealing at 600 °C for 100 s; (red) P spin-on-dopant in p-type Ge, following diffusion annealing at 600 °C for 600 s.

p- and n-type doped structures in Ge. The average etch rate for P-doped Ge was 19.5 nm/min and was slightly lower for B-doped Ge, at 18.7 nm/min. The slight decrease in etch rate for p-type Ge is apparent in Fig. 2(a), for depths >550 nm, where the doping changes from n- to p-type. Similarly, a slight increase in etch rate is apparent in Fig. 2(b) at depths >25 nm where doping changes from p- to n-type. The etch rates presented here are comparable with those of Brunco *et al.*,[5] which also showed a slightly higher etch rate in n-type Ge. Determining the average etch rate is significant since it gives an indication of the depth resolution that is possible when profiling. Since the etch rate is determined as ~20 nm/min it is both controllable—and therefore suitable for ultra-shallow doping—but is also fast enough to characterise deeper doping structures, i.e., in less than 1 h. Fig. 2 also states the standard deviation of each etch rate, which is 0.7 nm/min and 0.8 nm/min for P- and B-doped Ge, respectively. That is, the etch rate is adequately linear throughout the etching process. In light of this, and with the difference in etch rate only 4% between n- and p-type regions, it is apparent that the chemical etching method is suitable for differential Hall measurements of junctions in Ge.

Prior to differential Hall profiling, photolithography was used to fashion samples into a cloverleaf-shaped structure. Samples were characterized electrically according to the Van der Pauw principle[6] to determine sheet resistance, R_S. Carrier density and Hall mobility were realised using Hall-effect measurements, which provides the Hall coefficient, RHs. Hall measurements were carried out using a permanent magnet, creating a 0.3 T magnetic field. Successive rounds of resistance and Hall measurements were carried out following a cycle of etching. Between measurements, samples underwent etching for a time of between 3 s and 60 s depending on the desired depth resolution. The total etched depth was measured following profiling and the number of data points divided by the total etched depth to determine the spacing between each data point. By comparing the difference in measured R_S and RHs values before and after each removal, the carrier concentration and associated mobility profile can be deduced in the etched layer providing the depth of material removed is known. If each etched layer has a thickness δx, then the conductivity, σ, of the layer is $\sigma = \delta\sigma_S/\delta x$, where $\delta\sigma_S$ is the difference in sample conductivity before and after the layer is removed. The Hall coefficient of the removed layer can be derived as[7]

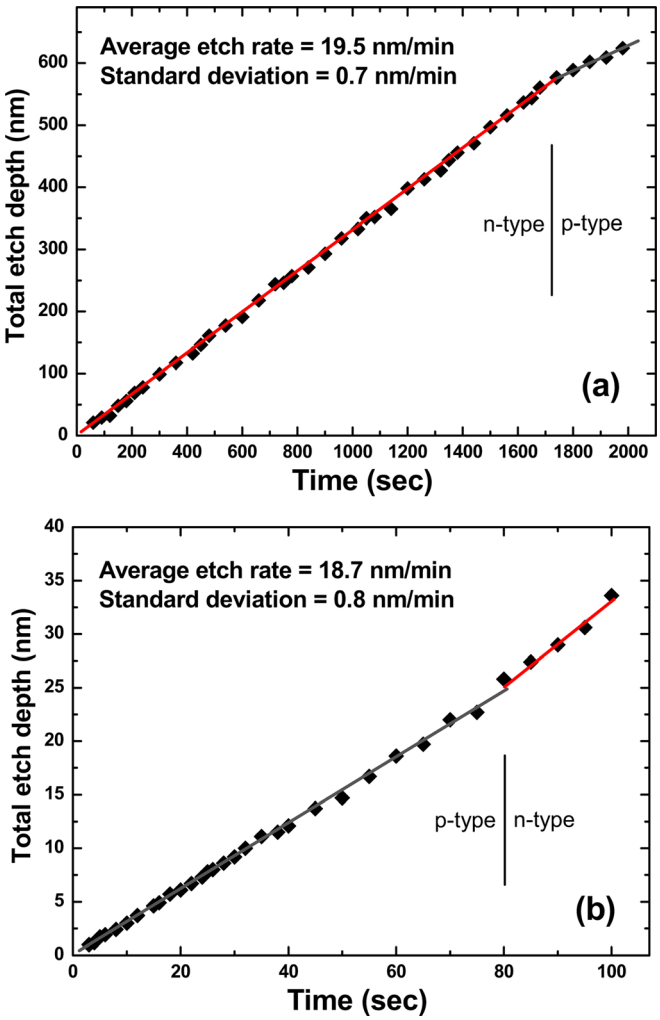

FIG. 2. Total etched depth during profiling plotted as a function of etch time for (a) P-doped p-type Ge and (b) B-implanted n-type Ge. In each case, the average etch rate and standard deviation is given. Lines are drawn as a guide to the eye, illustrating the different etch linearity in p-type (grey) and n-type (red) regions.

$$RHs\sigma^2 = \frac{\delta(RHs\sigma_S^2)}{\delta x}. \quad (1)$$

Since $\sigma = R_S{}^{-1}$, the Hall mobility, μ_H, of the removed layer can be expressed as

$$\mu_H = \frac{RHs}{R_S} = RHs\sigma = \frac{\delta(RHs\sigma_S^2)}{\delta\sigma_S}, \quad (2)$$

and since also $\sigma = e\mu_H N$, the concentration of carriers, N, in the removed layer is given by

$$N = \frac{\sigma}{e\mu_H} = \frac{(\delta\sigma_S)^2}{e\delta x.\delta(RHs\sigma_S^2)}, \quad (3)$$

where e is electronic charge.

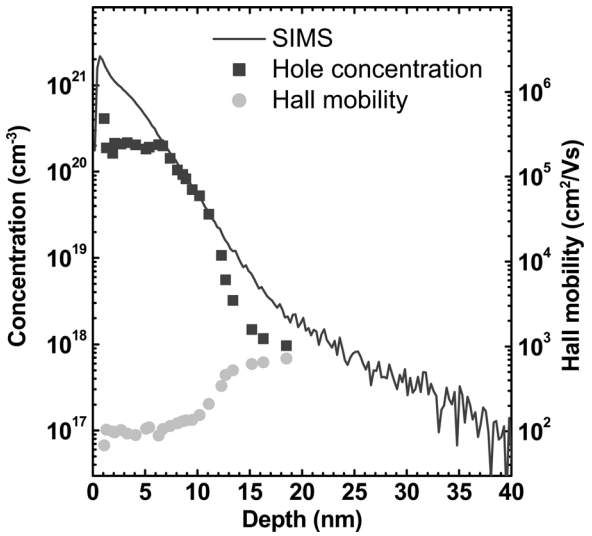

FIG. 3. Hole concentration and Hall mobility profiles as a function of depth for ultra-shallow B-doped Ge measured using the differential Hall technique. The carrier profile is compared to SIMS data. Hall data are corrected using a scattering factor equal to 1.2.

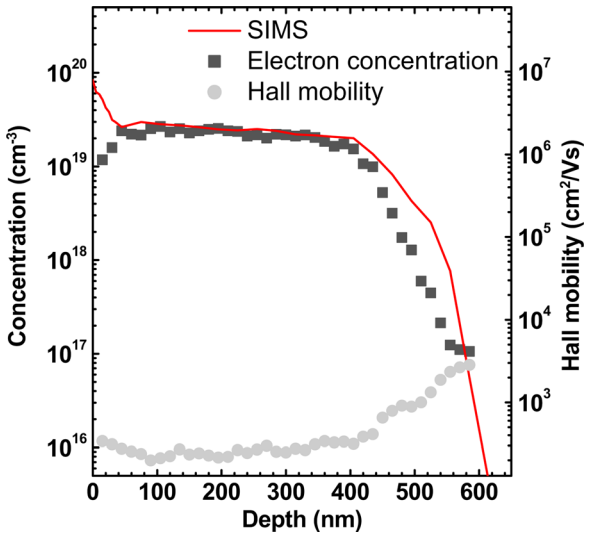

FIG. 4. Electron concentration and Hall mobility profiles as a function of depth for P-doped Ge measured using the differential Hall technique. The carrier profile is compared to SIMS data.

In Fig. 3, independent carrier and mobility profiles for ultra-shallow B-doped Ge are presented, measured using the differential Hall technique.[8] The profiles consist of data points with better than nanometre resolution. Differential Hall demonstrates that following annealing at 600 °C, the B activation level in Ge is $\sim 2 \times 10^{20}\,\mathrm{cm}^{-3}$. This value is in good agreement with the findings of Satta *et al.*[9] The necessary presence of a magnetic field in order to make a Hall measurement can provoke varying degrees of carrier scattering that distort the measured carrier concentration and Hall mobility, requiring a correction factor. A Hall scattering factor of 1.2 is applied to Hall data for B-doped Ge presented in Fig. 3, based on the findings of Mirabella *et al.*[10] This would seem a suitable choice based on the good agreement of SIMS and Hall data in the tail of the doping profile at 7–11 nm (Fig. 3). Beyond 11nm, the agreement between SIMS and Hall data is less good, the electrical data falling to lower values at any given depth. This is expected as profiling approaches the p-n junction and carriers are consumed by the depletion region. Fig. 3 also shows the Hall mobility profile for B-doped Ge. Mobility values as a function of concentration, $\mu(N)$, are in good general agreement with the findings of Golikova *et al.*[11]

In Fig. 4, independent carrier and mobility profiles for P-doped Ge are presented. In this case, a depth resolution of $\sim$20 nm is used as a compromise between adequate resolution and short measurement time. For P-doped Ge, the scattering factor is left as unity since the Hall factor for electrons is not forthcoming in contemporary scientific literature. A value of unity is however reasonable for two reasons: 1) it gives excellent agreement between the SIMS and electrical data; and 2) long-standing studies suggest that the ratio of Hall/conductivity mobility in n-Ge (an estimate of the Hall factor) is 1.05.[12] For P-doped Ge, as was the case for B-doped Ge, there is good agreement between the shape of the SIMS and electrical doping profiles. The P activation is lower than the SIMS concentration in the near-surface region, possibly due to an excess of vacancies close to the surface causing P deactivation.[13] As was the case for the B Hall profile, the tail of the P electrical profile is slightly shorter than the chemical profile, as expected. For the mobility data, $\mu(N)$ values are in good agreement with those found by Fistul *et al.*[14]

In conclusion, this Letter has demonstrated the application of the differential Hall technique for both microelectronic- and PV-relevant doping structures in Ge. Controllable and uniform layer removal was achieved with tailored depth resolution (<1–20 nm) for widely different doping structures (30 and 600 nm deep) of both p- and n-type. Slow chemical etching was used for layer removal—consisting of an etch solution containing one part H_2O_2 in ten parts deionised H_2O—to overcome issues associated with anodic oxidation and electrochemical profiling. The differential Hall technique provides an advantage over some other measurements since it is capable of separating the relative carrier concentration and mobility contributions to the conductivity of the doped layer under test. These factors combine to give rise to a technique capable of accurately determining dopant carrier and mobility profiles as a function of depth for doped Ge layers.

[1]K. T. Alavi, A. N. M. M. Choudhury, C. G. Fonstad, and J. C. Gelpey, Appl. Phys. Lett. **43**, 505 (1983).
[2]S. Prussin and J. Reyes, ECS Trans. **25**, 139 (2009).
[3]S. V. Hattangady, E. H. Nicollian, and R. J. Markunas, J. Electrochem. Soc. **134**, 1581 (1987).
[4]E. Garralaga Rojas, H. Plagwitz, B. Terheiden, J. Hensen, C. Baur, G. La Roche, G. F. X. Strobl, and R. Brendel, J. Electrochem. Soc. **156**, D310 (2009).
[5]D. P. Brunco, B. De Jaeger, G. Eneman, J. Mitard, G. Hellings, A. Satta, V. Terzieva, L. Souriau, F. E. Leys, G. Pourtois, M. Houssa, G. Winderickx, E. Vrancken, S. Sioncke, K. Opsomer, G. Nicholas, M. Caymax, A. Stesmans, J. Van Steenbergen, P. W. Mertens, M. Meuris, and M. M. Heyns, J. Electrochem. Soc. **155**, H552 (2008).
[6]L. J. Van der Pauw, Philips Res. Rep. **13**, 1 (1958).
[7]S. R. Blight, R. E. Nicholls, S. P. S. Sangha, P. B. Kirby, L. Teale, S. P. Hiscock, and C. P. Stewart, J. Phys. E: Sci. Instrum. **21**, 470 (1988).
[8]N. S. Bennett, A. J. Smith, B. Colombeau, R. Gwilliam, N. E. B. Cowern, and B. J. Sealy, Mater. Sci. Eng. B **124**, 305 (2005).

[9]A. Satta, E. Simoen, T. Clarysse, T. Janssens, A. Benedetti, B. De Jaeger, M. Meuris, and W. Vandervorst, Appl. Phys. Lett. **87**, 172109 (2005).
[10]S. Mirabella, G. Impellizzeri, A. M. Piro, E. Bruno, and M. G. Grimaldi, Appl. Phys. Lett. **92**, 251909 (2008).
[11]O. A. Golikova, B. Ya. Moizhez and L. S. Stilbans, Sov. Phys. Solid State **3**, 2259 (1962).
[12]F. J. Morin, Phys. Rev. **93**, 62 (1954).
[13]A. R. Peaker, V. P. Markevich, B. Hamilton, I. D. Hawkins, J. Slotte, K. Kuitunen, F. Tuomisto, A. Satta, E. Simoen, and N. V. Abrosimov, Thin Solid Films **517**, 152 (2008).
[14]V. I. Fistul, M. I. Iglitsyn, and E. M. Omelyanovskii, Sov. Phys. Solid State **4**, 784 (1962).